

# We are IntechOpen, the world's leading publisher of Open Access books Built by scientists, for scientists

**5,000**

Open access books available

**125,000**

International authors and editors

**140M**

Downloads

Our authors are among the

**154**

Countries delivered to

**TOP 1%**

most cited scientists

**12.2%**

Contributors from top 500 universities



**WEB OF SCIENCE™**

Selection of our books indexed in the Book Citation Index  
in Web of Science™ Core Collection (BKCI)

Interested in publishing with us?  
Contact [book.department@intechopen.com](mailto:book.department@intechopen.com)

Numbers displayed above are based on latest data collected.

For more information visit [www.intechopen.com](http://www.intechopen.com)



# Control and Dynamic Simulation of Linear Switched Reluctance Generators for Direct Drive Conversion Systems

*Rui Pedro Gouveia Mendes, Maria do Rosário Alves Calado and Sílvio José Pinto Simões Mariano*

## Abstract

This chapter addresses the dynamic simulation and control of linear switched reluctance generators for direct drive conversion systems. The electromechanical energy conversion principles of linear switched reluctance machines are briefly explained. A detailed mathematical model is developed for linear switched reluctance generators. The different types of control strategies adopted for switched reluctance generators are referred. The hysteresis controller is applied to control the conversion system with constant damping load. The proposed control strategy also includes a DC/DC isolated converter to control the system DC bus voltage by adjusting the energy flow between the conversion system and the resistive load. The mathematical model is applied to simulate the behavior of a tubular linear switched reluctance generator as power take-off system in an ocean wave point absorber device. To accomplish this task, the dynamic equations of the point absorber are presented and integrated with the linear switched reluctance generator dynamic model. In the simulation process, the system is driven by a regular ocean wave and operates with constant damping load. The system performance is evaluated for different load values, and the simulation results are presented for the optimal damping load case scenario.

**Keywords:** tubular linear generator, switched reluctance machine, direct drive conversion, ocean wave energy

## 1. Introduction

The switched reluctance machine (SRM) is an electromechanical structure with salient poles defined by a fixed and a movable part as the main constitutive elements. This machine is characterized by the absence of permanent magnets and by the electric phase coils only being present in just one part (usually the fixed part). The part where the phase coils are located is designed as primary and the other part, which works as passive element, as secondary. The SRMs can be rotating or linear. Since these two configurations are homologous, they share the same operation principles with the exception of the electromagnetic force direction [1]. In SRMs, a force is developed when the magnetic structure tends to minimize the magnetic energy by displacing the movable part to achieve a configuration with minimum

reluctance. This type of machine is characterized by a nonlinear electromagnetic behavior and can work as actuator or generator when the electric phase is energized during the period of increasing or decreasing inductance, respectively [2]. The SRM may have a flat structure [3] or a tubular one [4]. The tubular topology may overcome some disadvantages of the flat machine. The former has no edge effects due to the closed geometry. Also, the radial attraction forces are canceled due to its axisymmetric configuration [5].

This type of machine is suitable for low-speed applications and is a robust and low-cost solution since no permanent magnets are required for its operation. Also, the energy losses from Joule effect occurs in just one part and can, therefore, be more easily dissipated [6]. These characteristics make the SRM a strong candidate for generator in direct drive conversion systems. It has already been adopted as linear generator for ocean wave point absorbers [3]. Due to their unique advantages, the application of linear switched reluctance generators (LSRG) in direct drive conversion systems is of significant importance. Thus, design tools are necessary to develop and evaluate this type of machines, and suitable control techniques must be applied to ensure its reliable operation.

The aim of this chapter is to present the mathematical model to assist the design and assessment of LSRG. Also, control techniques are proposed for low-velocity operation. The mathematical formulation is applied to simulate the performance of a tubular linear switched generator (TLSRG) operating as a power take-off system in an ocean wave point absorber converter.

## 2. Electromagnetic conversion principles

In SRM, the magnetic circuit of each electric phase may be characterized with different values of magnetic reluctance for distinct relative positions of the movable part, in respect to the static part. When a magnetic field is established in this circuit, an electromagnetic force is developed to displace the movable part to the position with minimum magnetic reluctance in order to minimize the energy in the system. The referred position, designed as alignment position  $z_a$ , is characterized by the structural configuration where the saliencies of the movable part are aligned with the saliencies of the static part. In this situation, the self-inductance of the electric phase may achieve its maximum value. The nonalignment is verified for all the remaining relative positions, between the movable and static parts. For these

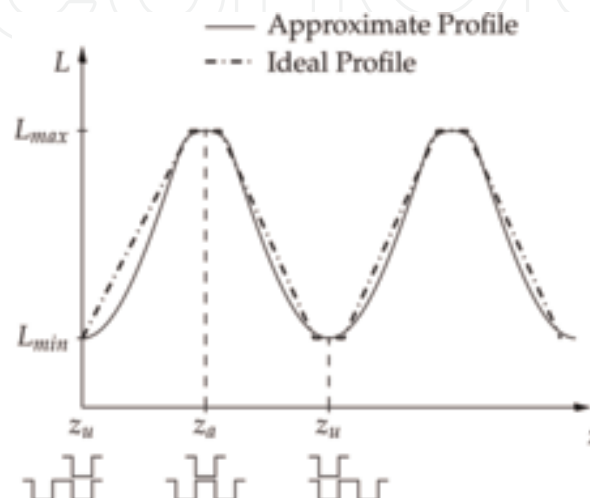


**Figure 1.**  
Typical inductance profile for SRMs.

configurations, the magnetic circuit of the electric phase is characterized by superior magnetic reluctance achieving its maximum value at the unaligned position  $z_u$ . This position is defined by the minimum value of inductance for the electric phase.

The typical linear inductance profile for SRMs is displayed in **Figure 1**. The inductance is given as function of the relative position between the movable and fixed parts. As consequence of the structural pattern inherent to these machines, when the movable part is moved in a single direction, the inductance is characterized by a periodic and symmetrical profile resulting from successive movements, which are approaching (the rate of change of the inductance  $L$  is positive) and leaving (the rate of change of the inductance  $L$  is negative) from the alignment position.

By energizing the electric phases in the approximation region or separation region, the SRM may operate as an actuator or a generator, respectively. In the first case, magnetic flux established by the electric phase will tend to minimize its energy developing an electromechanical force to achieve structural alignment. As a result, a linear force will act on the machine's movable part. In the presence of an external load, which can overcome the referred electromagnetic force, the generator is displaced from the alignment position, increasing the reluctance of the active phase, which will reduce the respective magnetic flux. As a consequence, a back-electromotive force is developed, seeking to increase the electric current to restore the magnetic flux. During this procedure, mechanical energy is extracted from the movable part of the generator and converted to electrical energy [7].

The electric phase equation is given as:

$$\begin{aligned} u_k &= R_a i + \frac{d\lambda}{dt} \\ &= R_a i + L(i, z_k) \frac{di}{dt} + i \frac{dz_k}{dt} \frac{dL(i, z_k)}{dz_k} \end{aligned} \quad (1)$$

where for phase  $k$ ,  $u_k$  is the voltage across the electric phase,  $R_a$  is the internal electric resistance,  $\lambda$  is the flux linkage,  $i$  is the electric current, and  $z_k$  is the electric position. In the last part of Eq. (1), *emf* is the back-electromotive force developed by the phase:

$$emf = i \frac{dz_k}{dt} \frac{dL(i, z_k)}{dz_k} = iv \frac{dL(i, z_k)}{dz_k} \quad (2)$$

with  $v$  as the velocity of the movable part of the linear SRM.

These conversion processes may only occur with appropriate power electronic converter to control the energy flow. With proper switch commands, the conversion periods may be established, and electric phase current intensity may be regulated by the converter [8].

In [9, 10], several electronic converters are identified that are suitable for electric generation with SRMs. The asymmetric H-bridge converter is the typical choice. This converter topology can be found, for one phase, in **Figure 2**. It is a practical and simple solution, but it is characterized with a variable output voltage due to the self-excitation process. However, this drawback may be minimized with an external voltage source [11]. This converter has the less apparent power required to operate and is classified as an economical solution [10].

With the converter illustrated in **Figure 2**, the conversion cycle may be defined by the excitation period, the generation period, and the free-wheeling period, an intermediate stage between the first two. The circuit configurations for the different periods are illustrated in **Figure 3**. Assuming that the capacitor is already at its nominal operating voltage, the excitation period is initiated when the switches  $S_1$

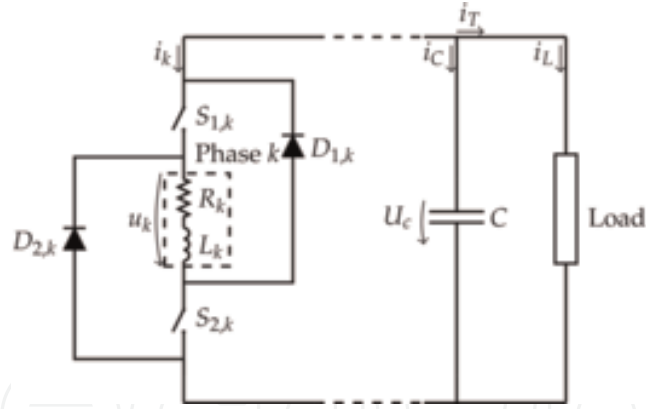


**Figure 2.** H-bridge asymmetric electronic power converter for one electric phase.

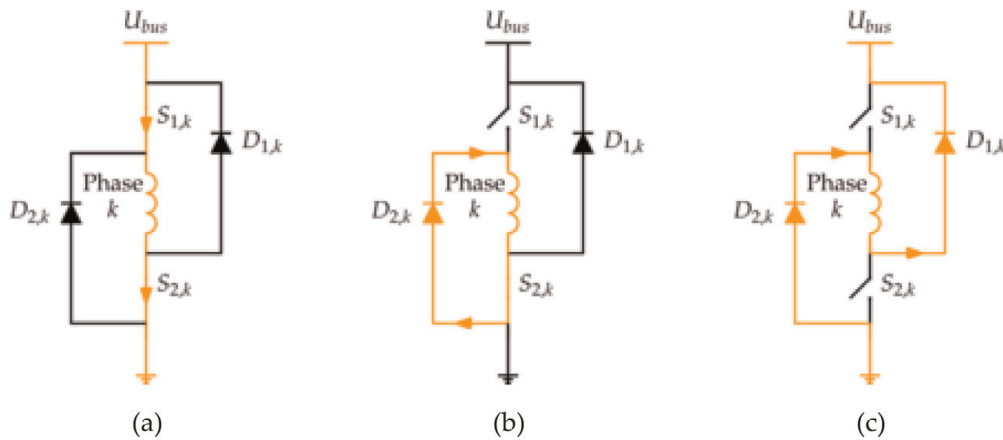


**Figure 3.** Circuit configuration and electric current path for (a) excitation period, (b) generation period, and (c) free-wheeling period (adapted from [12]).

and  $S_2$  are closed. Usually, this occurs when the phase is near the position that corresponds to its maximum inductance.

When the current intensity reaches a certain value, the switches are opened and the generation period begins. During this period, the back-electromotive force increases the electric current as a consequence of the magnetic flux reduction. Thus, the electric current is maintained through the diodes  $D_{1,k}$  and  $D_{2,k}$ , delivering the generated electric energy to the capacitor and to the load. The transition between these two conversion periods is characterized by hard commutation because the voltage is inverted. In the free-wheeling period, just one switch is closed to provide a zero voltage across the generator electric phase. Only the back-electromotive force acts on the phase electric current. This period can be implemented to achieve a soft commutation where, after the excitation period, the voltage is first annulled and, only then, inverted [12]. In each conversion cycle, the electric energy supplied by the converter during the excitation period is given by:

$$W_{exc} = \int_{t_{on}}^{t_{off}} ui \, dt \quad (3)$$

where  $t_{on}$  is the start time of the excitation period and  $t_{off}$  is the respective finish time.

The electric energy returned by the phase to the converter is:

$$W_{out} = \int_{t_{off}}^{t_{ext}} ui \, dt \quad (4)$$

with  $t_{ext}$  as the time when the electric current is extinguished. The amount of electric energy generated by the electromechanical conversion process is computed as follows:

$$W_{gen} = W_{out} - W_{exc} \quad (5)$$

### 3. Dynamic model

To assess the dynamic characteristics of switched reluctance generator, a mathematical model must be formulated to describe the system behavior in transient state. The mathematical model can be solved with numerical methods and computational calculus in order to estimate the system response for the given operating conditions. The mathematical model of SRMs is obtained from Eq. (1) that describes the transient phenomena involved in the electromagnetic conversion of each electric phase. The solution for this equation may be obtained by applying time integration to the linkage magnetic flux [13] or to the electric current derivative with time [14]. For both methods, it is required to relate the machine electromagnetic characteristics with the phase electric current and the movable part position. Several approaches have been proposed in the literature to include the machine nonlinear nature in the mathematical model. In [15], look-up tables are used to model the electromagnetic characteristics of the SRM. These are obtained from a static analysis and are used as data base to build the look-up tables. Analytic functions are also used to represent the machine magnetic characteristics within the mathematical model. The use of analytical expressions simplifies the computation process related to the differentiation and integration of the electromagnetic entities [16]. This approach can be achieved by fitting an appropriate function to discrete data [17]. Fourier series expansion may also provide analytical expressions to represent nonlinear electromagnetic characteristics in the SRM mathematical model [18]. A simpler method, but less precise, comprises the use of piecewise functions to establish a linear [19] or nonlinear [20] relation with the independent variables. Artificial intelligence-based methods have already been adopted in the dynamical analysis of SRMs. These methods comprise the use of neural networks and fuzzy logic with real data to develop a mathematical representation of SRM electromagnetic characteristics [21].

All the referred approaches require the representative data of the electromagnetic characteristics, usually expressed as a function of the electric phase current intensity and movable part relative position. With look-up tables, these data are used directly. Methods based on analytic expressions or artificial intelligence models apply these data to develop appropriate mathematical expressions.

The required discrete data may be obtained through experimental measurements. This process provides realistic curves, but a physical model of the machine is needed for it. In electric machine design, where several structural possibilities must be assessed, it becomes unpractical to get the machine electromagnetic characteristics with experimental evaluation, as numerical or analytical methods are needed to perform this task. As an alternative to experimental tests, the finite element method

(FEM) is used for electromagnetic characterization of SRMs, providing results with great precision, but needing for a sophisticated mathematical implementation and large amount of computational resources to process the solution [22]. However, with the existence of FEM-based commercial software, it is possible to evaluate electromagnetic systems without a deep knowledge of electromagnetism. Thus, FEM is getting more adopted in the design of electric machines.

The mathematical model of switched reluctance generator results from the analysis of the associated power converter. Since all electric phases are defined by identic magnetic and electric circuits, they are represented by the same dynamic equations. Its analysis is generalized following the notation specified in **Figure 2**. The voltage across each electric phase  $k$  is:

$$u_k = R_{a_k} i_k + \frac{d\lambda_k}{dt} \quad (6)$$

where for each phase  $k$ ,  $R_{a_k}$  is the internal electric resistance,  $i_k$  is the electric current,  $\lambda_k$  is the magnetic linkage flux, and  $z_k$  is the electric position. The magnetic linkage flux is given by:

$$\lambda_k = \sum_{j=1}^q \lambda_{kj}(z_j, i_j) \quad (7)$$

with  $\lambda_{kj}(z_j, i_j)$  as the magnetic linkage flux in phase  $k$  due to current in phase  $j$  and  $q$  as the number of electric phases. Replacing Eq. (7) in Eq. (6):

$$u_k = R_{a_k} i_k + \lambda_k = \sum_{j=1}^q \frac{d\lambda_{kj}(z_j, i_j)}{dt} \quad (8)$$

Applying the chain rule to Eq. (8), one has:

$$u_k = R_{a_k} i_k + \left( L_k(z_k, i_k) + i_k \frac{dL_k}{di_k}(z_k, i_k) \right) \frac{di_k}{dt} + v i_k \frac{dL_k}{dz_k}(z_k, i_k) + \sum_{\substack{j=1 \\ j \neq k}}^q \left[ \left( M_{kj}(z_j, i_j) + i_j \frac{dM_{kj}}{di_j}(z_j, i_j) \right) \frac{di_j}{dt} + v i_j \frac{dM_{kj}}{dz_j}(z_j, i_j) \right] \quad (9)$$

where  $L_k$  is the self-inductance of phase  $k$  and  $M_{kj}$  is the mutual inductance between phases  $k$  and  $j$ . The linear velocity of the movable part  $v$  is:

$$v = \frac{dz_k}{dt} = \frac{dz_j}{dt} \quad (10)$$

The electromotive force, which results from the change of magnetic flux in phase  $k$ , is:

$$emf_k = v \left[ i_k \frac{dL_k}{dz_k}(z_k, i_k) + \sum_{\substack{j=1 \\ j \neq k}}^q i_j \frac{dM_{kj}}{dz_j}(z_j, i_j) \right] \quad (11)$$

During the conversion period, electric energy is exchanged between the capacitor of the converter and the electric phases of the generator. In the excitation period, the capacitor supplies energy to the phase and in the generation period receives energy from it. The voltage across capacitor  $U_c$  is related with its capacity and input current  $i_c$  by:

$$i_c = C \frac{dU_c}{dt} \quad (12)$$

The total net value of the electric energy flowing between the electric phases and the capacitor  $i_T$  is given by:

$$i_T = \sum_{j=1}^q i_k \quad (13)$$

The bus voltage  $U_{bus}$  of electronic power converter is imposed by capacitor voltage:

$$U_{bus} = U_c \quad (14)$$

In order to fully define the model of the switched reluctance generator system, the voltage across each electric phase must be known. Its value depends on the different circuit configurations for the electric energy flow in the phase. According to the possible combinations of switch states, there are three different configurations, as illustrated in **Figure 3**, each of them corresponding to a distinct period of electromagnetic conversion.

The voltage across each electric phase, according to the switch states, is:

$$u_k = \begin{cases} U_{bus} - 2U_s & S_{1,k} \text{ and } S_{2,k} \text{ closed} \\ -U_{bus} - 2U_D & S_{1,k} \text{ and } S_{2,k} \text{ open} \\ -U_D - 2U_s & S_{1,k} \text{ open and } S_{2,k} \text{ closed} \end{cases} \quad (15)$$

with  $U_s$  and  $U_D$  as the voltage drops across the electronic switch and diode, respectively.

The linear force exerted by the generator  $F_{gen}$  is:

$$F_{gen}(t) = \sum_{k=1}^q F_{em,k}(z_k, i_k) \quad (16)$$

where  $F_{em,k}(z_k, i_k)$  is the individual component of force provided by electric phase  $k$  during the conversion cycle. The generator electric efficiency can be determined by the mean values of the generated electric power  $\bar{P}_{gen}$  and extracted mechanical power  $\bar{P}_{mec}$  as:

$$\eta_e = \frac{\bar{P}_{gen}}{\bar{P}_{mec}} \quad (17)$$

All the formulation presented so far was defined for a phase electric position falling within the two opposing nonalignment positions. As the movable part of the generator is displaced, the electric position describes a periodic profile which is identical in all electric phases of the SRM. However, these electric positions have



distinct values for the same absolute position because the phases are shifted. The relation between the electric position of one phase  $z_k$  and the mechanical absolute position  $z_{mech}$  is defined by:

$$z_k = -S_t + \left( \frac{z_{mech} - k_{offset} - S_t}{2S_t} - \left\lfloor \frac{z_{mech} - k_{offset} - S_t}{2S_t} \right\rfloor \right) 2S_t \quad (18)$$

where  $k_{offset}$  is the shift distance between the same electric position of two consecutive phases and  $S_t$  is the distance between the aligned and unaligned positions of the phase.

The graphical representation of Eq. (18) can be found in **Figure 4**.

The mathematical model of the LSRG system is defined by a nonlinear problem of initial value and is schematized in **Figure 5**. To obtain the respective solution, it is necessary to perform the time integration of the differential equations that govern the system electromechanical behavior. Also, a controller must be included to provide the appropriate switching commands to the electronic power converter.

The bus voltage of the LSRG converter should be kept as constant as possible to allow for a proper self-excitation operation. Also, since high voltage levels are required to energize each phase in due time, it may be desirable to reduce the output voltage applied to the electric load. To achieve these requirements, an H-bridge isolated DC/DC converter is admitted in the conversion system to control the energy flow between the conversion system and the electric load, as schematized in **Figure 6**. With the ideal model of the H-bridge isolated DC/DC converter, it is possible to establish a relation between the mean values of the input and output voltages ( $U_1$  and  $U_2$ ) and of the input and output currents ( $I_1$  and  $I_2$ ).

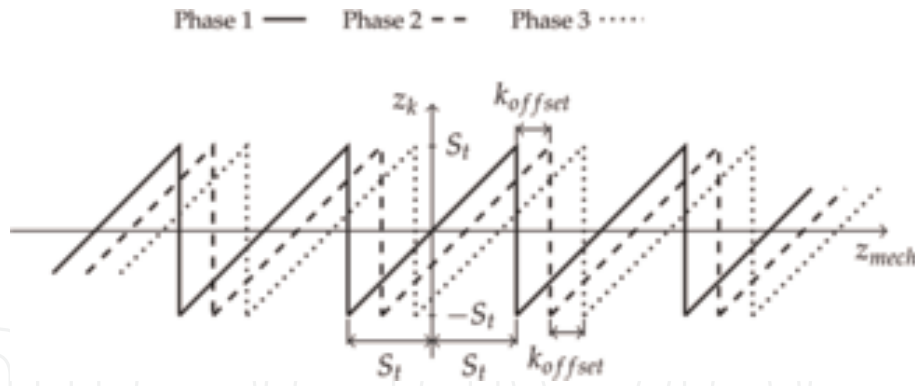


**Figure 4.**  
Electric position as function of mechanical position.

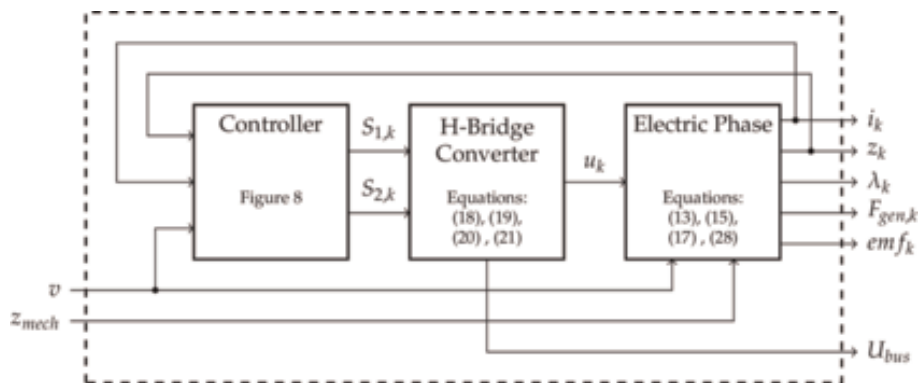


**Figure 5.**  
Diagram of the mathematical model of the LSRG system.

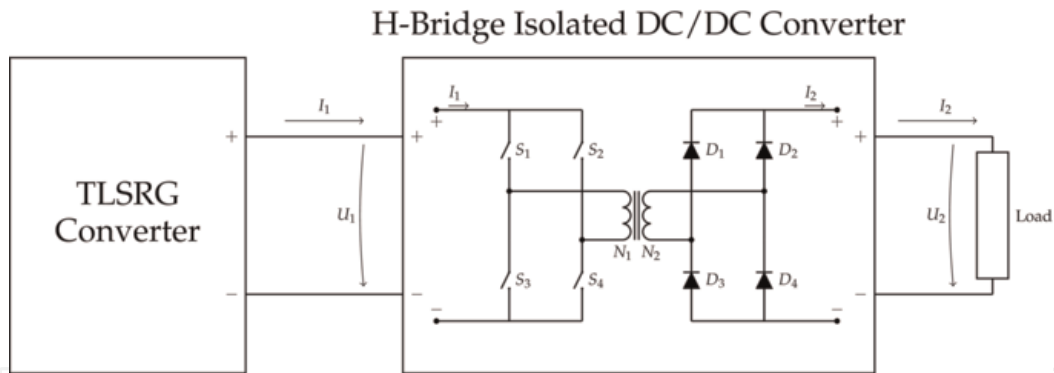


**Figure 6.**  
 TLSRG conversion system with a DC/DC conversion stage.

The duty cycle  $D$  is the control parameter to regulate the output voltage at constant chopping frequency. The relations between the referred electric entities are defined in [23] as:

$$\bar{U}_2 = 2\bar{U}_1 D \frac{N_2}{N_1} \quad (19)$$

$$\bar{I}_1 = 2\bar{I}_2 D \frac{N_2}{N_1} \quad (20)$$

where, respectively,  $\bar{U}_1$  and  $\bar{U}_2$  are the mean values of input and output voltages,  $\bar{I}_1$  and  $\bar{I}_2$  are the mean values of input and output electric currents, and  $N_1$  and  $N_2$  are the numbers of turns of the transformer primary and secondary coils.

#### 4. Control

The SRM operation relies on the switching electric positions. Fixed values for these positions may cause system instability, especially when operating at variable velocity. As a consequence, the converter bus voltage may change considerably, depending on the system electric load [24]. Therefore, a closed loop control is required. As stated in [25], when operating as generator, the control of SRMs must be applied to preserve the converter output voltage, conditioned by the current flow in the electric phases and electric load.

The amount of energy extracted for conversion relies on the electromechanical force exerted by the generator which is also affected by the electric phase current. Thus, with a proper switching strategy, it is possible to control the electric current intensity to attain a desirable voltage level as well as to improve the system conversion efficiency. With the additional DC/DC converter, the bus voltage may also be kept near a nominal value by modifying the energy flow between the LSRG converter and the load. This method is proposed in [24] to achieve maximum energy conversion by controlling the voltage level according to the velocity of the generator.

At low operation velocities, the back-electromotive force is inferior to the bus voltage and the current is forced to decrease gradually. In this situation, the phase must be submitted to successive commutations to adjust the applied voltage and achieve the desirable current intensity [7]. This process can be accomplished with hysteresis band control [26]. This control is characterized with a variable switching frequency because it is conditioned by the rate of change of the electric phase current [27].

The control of the switched reluctance generator is the selection of appropriate parameter values that are responsible for its behavior. For velocities superior to the

base velocity, it is only necessary to account the electric positions that define the conversion cycle. For lower velocities, it is also required to define a reference value for the phase current. With the mathematical model, it is possible to establish an optimal relation between the values of the control parameters and the physical entities that need to be controlled and include it in the control process through look-tables or fitted analytical expressions. Thus, the appropriate control parameters can be defined as function of the operation variables [28].

The proportional integral (PI) control may be applied to control the switched reluctance generator. It has been used in real-time optimal control of rotating generators, where the reference current and commutation angles are computed from the error of the output voltage [29]. PI control was adopted in [30] to adjust the phase current intensity and minimize the converter output voltage ripple in linear generators.

#### 4.1 Hysteresis control

With proper switching commands, the current is maintained within the hysteresis band  $h_b$ , which is a range of values established around the reference current  $i_{ref}$ . The typical current profile obtained with this control is shown in **Figure 7(a)**. When the current falls below the inferior limit of the hysteresis band  $-h_b/2$ , the phase is energized to increase the current. If it is superior to the upper limit of the hysteresis band  $h_b/2$ , the switches are opened and the generation period begins until the lower limit is reached again [31]. The phase current error  $e_i$  is used to control the switches in agreement with the logic schematized in **Figure 7(b)**.

The conversion cycle is characterized by successive excitation and generation periods that occur while the phase electric position is between  $z_{on}$  and  $z_{off}$  and the movable part is in motion. For zero velocity, there is no electric generation and the switches remain opened. Thus, for each phase  $k$ , the hysteresis controller provides the electronic switching commands  $S_{1,k}$  and  $S_{2,k}$  as a function of the phase electric position  $z_k$ , movable part velocity  $v$ , current reference value  $i_{ref}$ , hysteresis band  $h_b$ , and electric positions  $z_{on}$  and  $z_{off}$ . In **Figure 8** the algorithm of the hysteresis controller is illustrated. For an optimal control, the parameters must be chosen to maximize the generated electric energy. With the mathematical model of the conversion system, these parameters may undergo an optimization process to find the best values for the best performance.

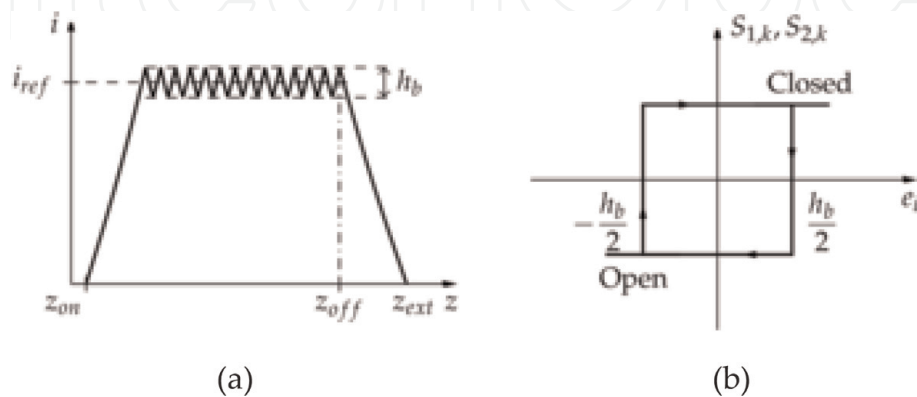


**Figure 7.** Hysteresis control: (a) electric current profile and (b) control logic.

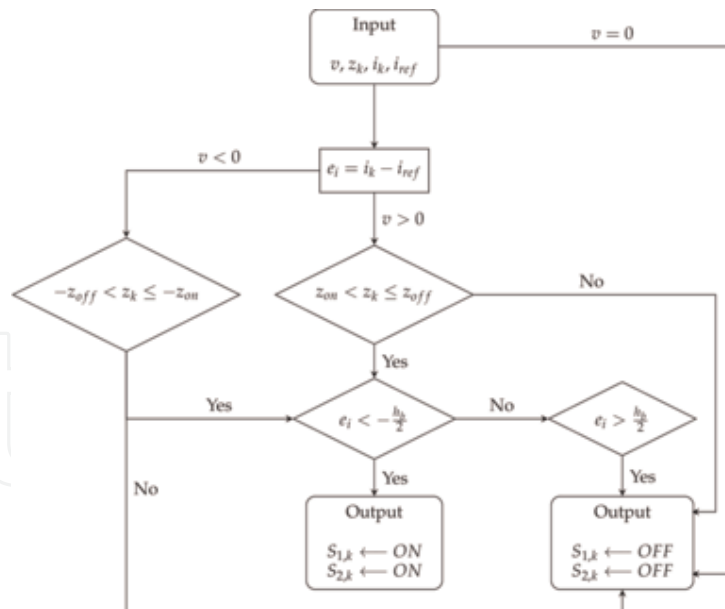


**Figure 8.**  
 Block diagram of algorithm proposed to apply the hysteresis control.

## 4.2 Proportional integral (PI) control

The H-bridge isolated DC/DC converter is used to maintain the system DC bus voltage level close to a reference value. In order to accomplish it, a PI control is used to properly compute the duty cycle value for the applied switching commands. The control variable  $s$  is given as function of error  $e$  between the variable to be controlled and the respective reference value:

$$s(t) = K_p e(t) + K_i \int_0^t e(\tau) d\tau \quad (21)$$

with  $K_p$  and  $K_i$  as the controller proportional and integral gains, respectively. The duty cycle value is given as:

$$D(t) = D_{init} + \Delta D(t) \quad (22)$$

where  $D_{init}$  is the initial value of the duty cycle and  $\Delta D(t)$  is the incremental duty cycle provided by the PI controller:

$$\Delta D(t) = K_p e_u(t) + K_i \int_0^t e_u(\tau) d\tau \quad (23)$$

with  $e_u$  as the normalized error between DC bus voltage  $U_{bus}$  and the reference value  $U_{ref}$ :

$$e_u(t) = \frac{U_{ref} - U_{bus}(t)}{U_{ref}} \quad (24)$$

## 5. Practical case study scenario

The described formulation will be applied to evaluate the performance of a tubular linear SRM working as generator in an ocean wave point absorber device schematized in **Figure 9**.

The system comprises a floating body that drives the generator by action of the incoming ocean waves. The linear generator is a three-phase machine with coils located in the inner part. The outer part is rigidly coupled to a floating body that only allows a vertical motion. Mechanical springs are used to link the generator outer part to the reference system, which is fixed to the ocean bottom. The tubular LSRG is illustrated in **Figure 10**.

### 5.1 Point absorber mathematical model

The mathematical model of an ocean wave direct drive converter is also needed to fully define the conversion system and to compute the mechanical entities that are used as input in the generator dynamic model.

The dynamic behavior of the point absorber device can be found in [32] and is described by the expression:

$$m_b \ddot{z} = F_{exc}(t) + F_{rad}(t) + F_H(t) + F_V(t) + F_{gen}(t) \quad (25)$$

where  $m_b$  is the combined mass of the floating body and generator movable part,  $\ddot{z}$  is the bodies' acceleration,  $F_{exc}$  is the wave excitation force,  $F_{rad}$  is the radiation force,  $F_H$  is the hydrostatic force,  $F_v$  is the viscous damping force, and  $F_{gen}$  is the generator damping force.

The excitation force is given by:

$$F_{exc}(t) = \Re \left[ S_a \tilde{F}_{exc}(\omega) e^{i(\omega t + \varphi)} \right] \quad (26)$$

with  $S_a$  as the wave amplitude,  $\tilde{F}_{exc}$  as the complex value of the excitation force per meter of wave amplitude,  $\omega$  as the wave angular frequency, and the  $\varphi$  as wave phase.

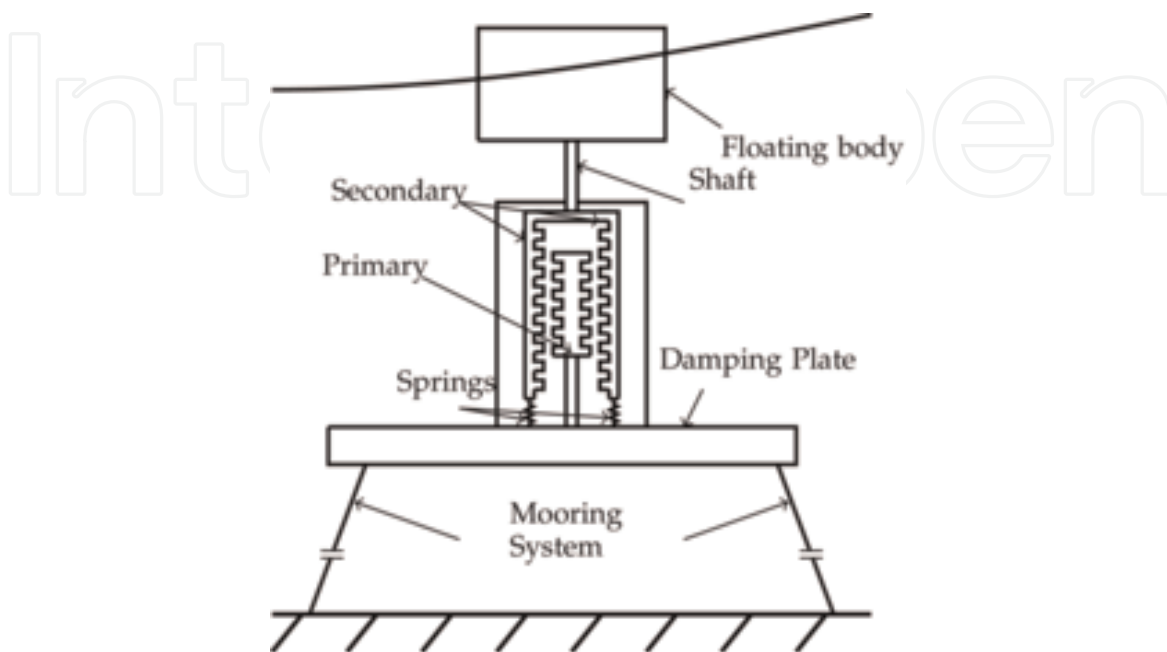


**Figure 9.**  
Point absorber schematics.

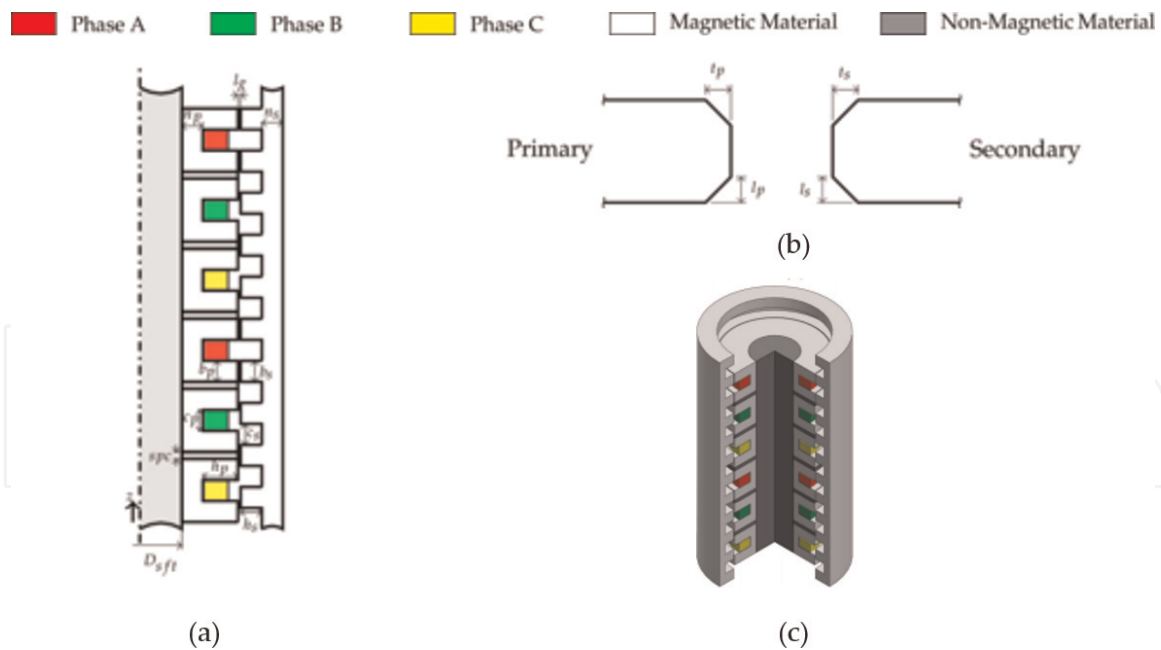


**Figure 10.** Tubular LSRG (TLSRG) used as PTO: (a) longitudinal cross-sectional profile, (b) tooth shape, and (c) 3D illustration.

The radiation force is calculated as follows:

$$F_{rad}(t) = -m_{\infty}\ddot{z} - \int_0^t K_r(t - \tau)\dot{z}(\tau) d\tau \quad (27)$$

In Eq. (27),  $m_{\infty}$  is the added mass for infinite frequencies,  $K_r$  is the radiation velocity impulse response, and  $\dot{z}$  is the floating body and generator movable part. The hydrostatic force is:

$$F_H(t) = -\rho g A_w z \quad (28)$$

with  $\rho$  as the specific mass of seawater,  $g$  as the gravity acceleration,  $A_w$  as the cross-sectional area of the submerged part of the floating body, and  $z$  as its vertical position.

The floating body is subjected to a viscous drag force given by:

$$F_V(t) = -\frac{1}{2}\rho C_D A_D |\dot{z} - \dot{\eta}|(\dot{z} - \dot{\eta}) \quad (29)$$

where  $A_D$  is the cross-sectional area of the floating body,  $C_D$  is the viscous drag coefficient, and  $\dot{\eta}$  is the vertical velocity of the water surface. The mathematical equations of TLSRG and the point absorber devices are combined to fully define the dynamic model for the direct drive ocean wave conversion system, as schematized in **Figure 11**.

## 5.2 System simulation/simulation results

A sinusoidal ocean wave with a period of 7.7 s and a height of 1.3 m was considered to drive the floating body of the point absorber. The floating body is cylinder with a diameter of 3.4 m and a vertical extension of 4.9 m. The TLSRG was designed with a mean damping force of 40 kN, which is the maximum load

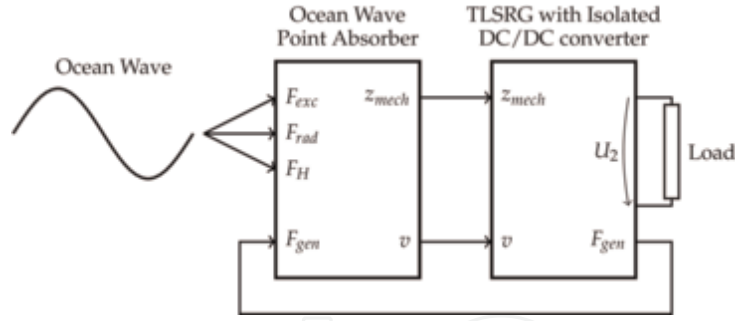


**Figure 11.** Schematics of the ocean wave conversion system dynamic model.

$l_g$ [mm]	$N_t$	$D_{sft}$ [mm]	$w_h$ [mm]	$w_v$ [mm]	$b_p$ [mm]	$c_p$ [mm]	$n_p$ [mm]	$h_p$ [mm]	$l_p$ [mm]	$t_p$ [mm]	$k_{offset}$ [mm]
5.1	230	499.5	0.1	1.7	170	152	222.4	46.7	13.9	9.3	107.3

**Table 1.** Dimensional parameters of the TLSRG.

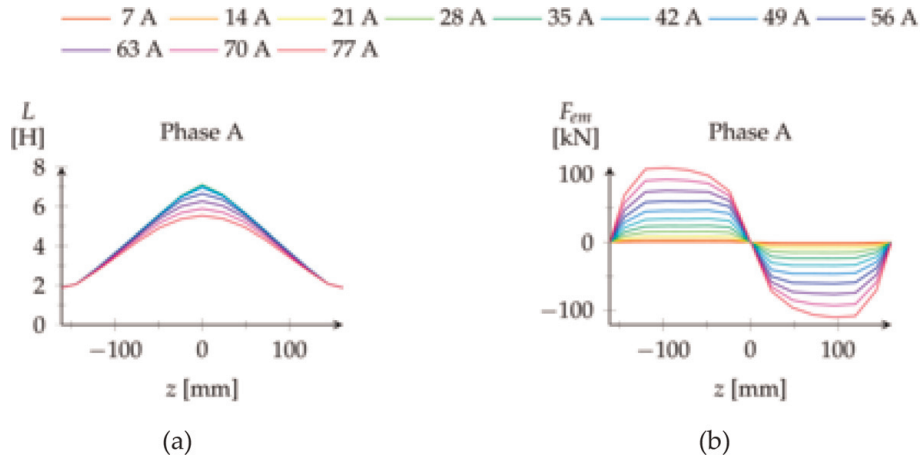


**Figure 12.** Electromagnetic characteristic for the electric phase A of TLSRG: (a) inductance and (b) axial force.

expected for the ocean wave considered for simulation. The dimensions of the TLSRG are presented in **Table 1**. The electromagnetic characteristics of the machine, displayed in **Figure 12**, were obtained with MagNet<sup>®</sup>, a commercial software that uses the finite element method for electromagnetic analysis. The control parameters  $h_b$ ,  $z_{on}$  and  $z_{off}$  were optimized for different combinations of velocity and phase current to maximize the mean value of the generated electric power. In this chapter, only the dynamic simulation of the system is important, so the applied optimization process is not presented. The optimal values are displayed in **Figure 13**.

These values were included in the mathematical model through 2D look-up tables and were computed, as function of the TLSRG movable part velocity and phase current, by linear interpolation. The capacitor in the converter was defined with a capacitance of 0.05 F.

A value of 41,430 kg was assumed for the mass of the oscillating body  $m_b$ , and the added mass for infinite frequencies  $m_\infty$  was quantified as 9951.1 kg. The specific mass of seawater  $\rho$  was set as 1025 kg/m<sup>3</sup>, and for the viscous drag coefficient, a value of 0.88 was defined. The excitation force profile and impulse response function were computed with NEMOH and are displayed in **Figure 14**. For the H-bridge

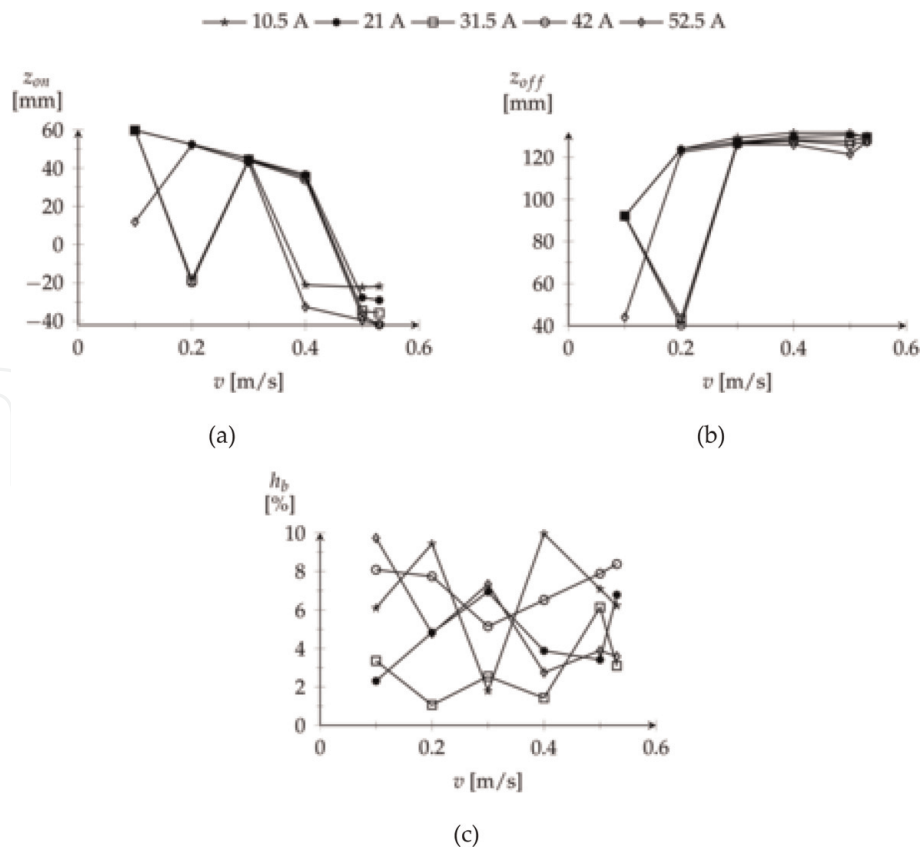


**Figure 13.** Optimal values for (a)  $h_b$ , (b)  $z_{on}$ , and (c)  $z_{off}$ .

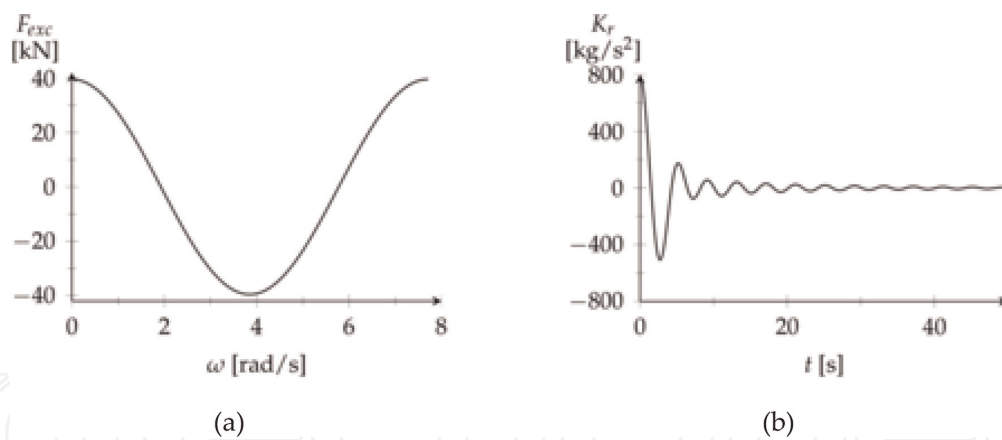


**Figure 14.** Wave-body interaction loads: (a) excitation force profile and (b) impulse response function.

isolated DC/DC converter, the ratio  $\frac{N_2}{N_1}$  was chosen as 10 to supply an output voltage of 400 V for a DC bus voltage of 4 kV and a duty cycle of 0.5. The PI controller was configured with a proportional gain  $K_p$  of 4089.3 and an integral gain  $K_I$  of 639.6. The system's mathematical model was implemented in Simulink<sup>®</sup> and was solved by the Dormand-Prince method, with a relative tolerance of  $1 \times 10^{-3}$  and a maximum step of  $8 \times 10^{-4}$  s. The system's mathematical model was simulated for distinct values of  $i_{ref}$  in order to evaluate the generator performance with different damping forces. The mean value of generated electrical power and electric conversion efficiency, as function of  $i_{ref}$ , can be found in **Figure 15**.

Attending to the simulation results, the greatest average of electric generated power was 7.6 kW for a reference current of 35 A. For this reference, current value



also had the best electric efficiency of 43%. **Figure 16** shows the oscillating body absolute position and velocity obtained from the simulations with  $i_{ref}$  of 35 A.

The electric phase current and electromechanical force profiles are shown, respectively, in **Figures 17** and **18**. The TLSRG converter DC bus voltage level is displayed in **Figure 19**. With the application of the DC/DC isolated converter, the DC bus voltage was kept near its reference value with a maximum error of 1.05%.

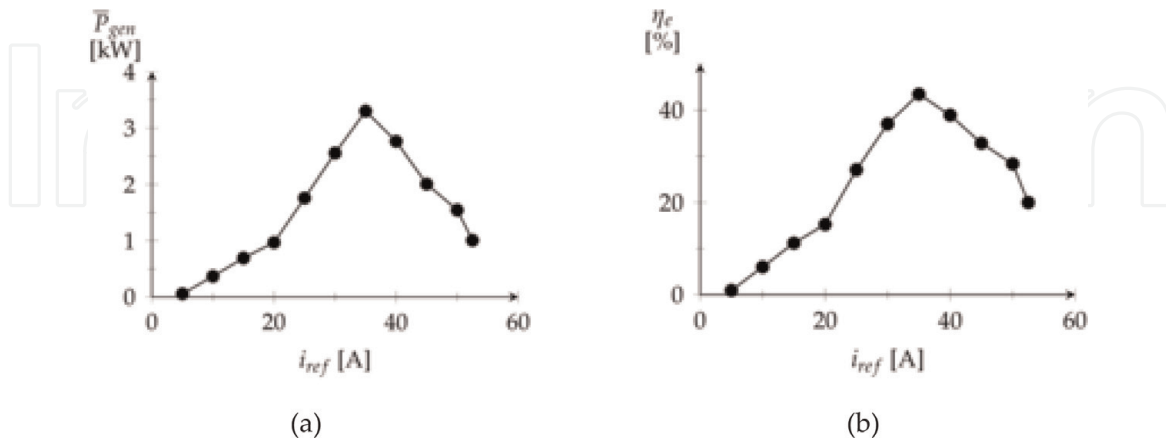


**Figure 15.** TLSRG performance for different values of  $i_{ref}$ : (a) mean value of generated electric power and (b) electric conversion efficiency.

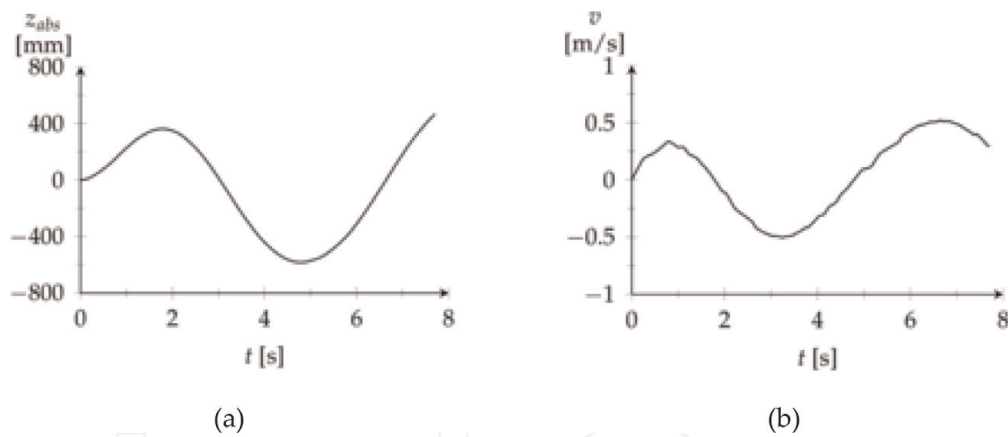


**Figure 16.** Oscillating body profile for (a) absolute position and (b) linear velocity.

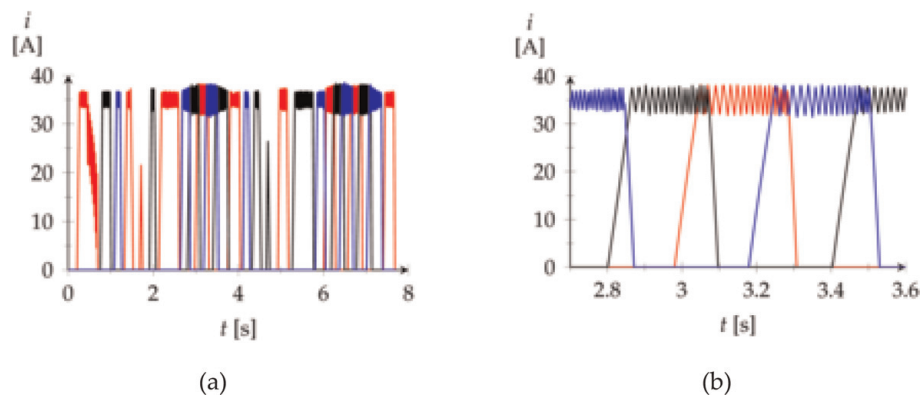


**Figure 17.** Electric current profile for each electric phase: (a) normal view and (b) zoomed view.

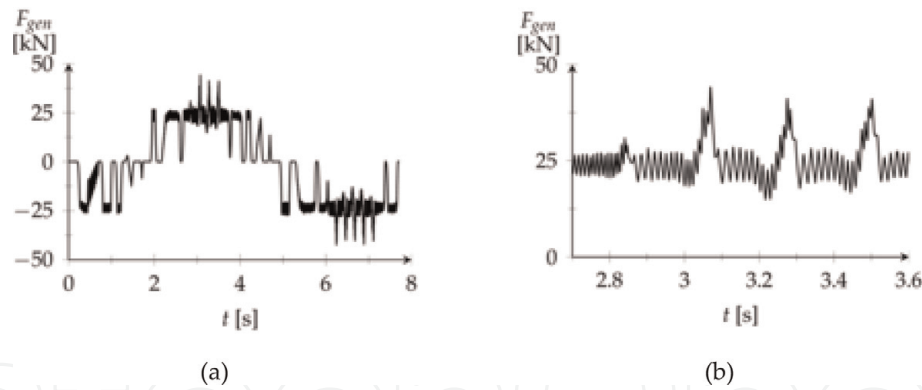


**Figure 18.**  
 Electromagnetic linear force profile: (a) normal view and (b) zoomed view.

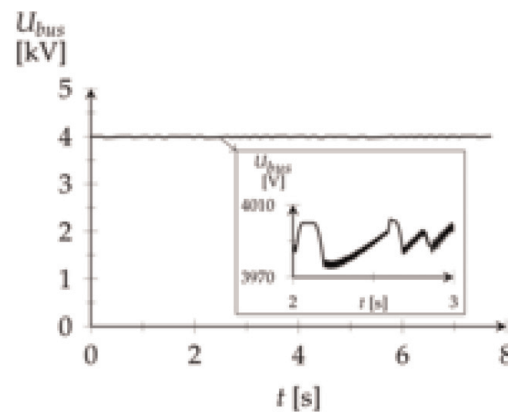


**Figure 19.**  
 TLSRG converter DC bus voltage.

## 6. Conclusion

In this chapter, a mathematical model to simulate the dynamic behavior of linear switched reluctance generators was presented, to apply in ocean wave direct drive converters. The model was developed according with the circuit configuration of the H-bridge asymmetric converter, adopted as power electronic converter to control the energy flow in the machine when operating as a generator. A hysteresis controller was applied to maintain the electric phase current close to a reference value during each conversion cycle, in order to allow the control of the generator damping force. Also, a DC/DC isolated converter was admitted to adjust the energy flow between the H-bridge asymmetric converter and the system electric load, in order to keep the DC bus voltage level near its nominal value. A PI controller was proposed to control the pulse width of the DC/DC conversion stage. A practical study case scenario was considered where the generator mathematical model was applied to simulate TLSRG operating as a power take-off system in an ocean wave point absorber device. The mathematical model of the TLSRG was integrated with the dynamic equations of the point absorber to evaluate the system behavior. In the simulation process, a regular ocean wave was assumed to drive the system. The system performance was evaluated for distinct values of  $I_{ref}$ , which implies distinct damping load profiles. The best performance was found for an  $I_{ref}$  of 35 A where an average electric power of 7.6 kW was generated with an efficiency of 43%. With the application of the DC/DC isolated converter, it was possible to maintain the DC bus voltage near its reference value with a maximum deviation of 1.05%.

## **Acknowledgements**

The authors wish to thank Instituto de Telecomunicações for funding this work, with the investigation scholarship UID/EEA/50008/2019 and research grant BPD/N°19—29/01/2019—UID/EEA/50008/2019.

IntechOpen

IntechOpen


### **Author details**

Rui Pedro Gouveia Mendes, Maria do Rosário Alves Calado  
and Sílvio José Pinto Simões Mariano\*  
University of Beira Interior and Instituto de Telecomunicações, Covilhã, Portugal

\*Address all correspondence to: [sm@ubi.pt](mailto:sm@ubi.pt)

### **IntechOpen**

---

© 2020 The Author(s). Licensee IntechOpen. Distributed under the terms of the Creative Commons Attribution - NonCommercial 4.0 License (<https://creativecommons.org/licenses/by-nc/4.0/>), which permits use, distribution and reproduction for non-commercial purposes, provided the original is properly cited. 

## References

- [1] Boldea I, Nasar S. *Linear Electric Actuators and Generators*. Cambridge, UK: Cambridge University Press; 2005
- [2] Méndez S, Martínez A, Montañó C, Millan W, Oyarbide E, Pérez F. Design and characterization of a 1 kW AC self-excited switched reluctance generator. In: *Proceedings of the IECON 2011—37th Annual Conference on IEEE Industrial Electronics Society*, Melbourne, Victoria, Australia. Piscataway, NJ: IEEE; 2011. pp. 1789-1794
- [3] Du J, Liang D, Xu L, Li Q. Modeling of a linear switched reluctance machine and drive for wave energy conversion using matrix and tensor approach. *IEEE Transactions on Magnetics*. 2010;**46**(6): 1334-1337
- [4] Llibre FJ, Martinez N, Nogarède B, Leprince P. Linear tubular switched reluctance motor for heart assistance circulatory: Analytical and finite element modeling. In: *2011 10th International Workshop on Electronics, Control, Measurement and Signals (ECMS)*, Liberec, Czech Republic. Piscataway, NJ: IEEE; 2011. pp. 1-6
- [5] Dio V, Miceli R, Trapanese M. The use of sea waves for generation of electrical energy: A linear tubular asynchronous electrical generator. In: *OCEANS 2007, Vancouver, British Columbia*. Piscataway, NJ: IEEE; 2007. pp. 1-4
- [6] Moreau L, Zaïm M, Machmoum M. Electromagnetic design optimization of a low speed Slotted Switched Reluctance Machine using genetic algorithm. In: *XXth International Conference on Electrical Machines (ICEM)*, Marseille, France. Piscataway, NJ: IEEE; 2012, 2012. pp. 233-237
- [7] Torrey D. Switched reluctance generators and their control. *IEEE Transactions on Industrial Electronics*. 2002;**49**(1):3-14
- [8] Lee D, Ahn J, Liang J. Classification and analysis of switched reluctance converters. *Journal of Electrical Engineering & Technology*. 2010;**5**(4): 571-579
- [9] Krishnan R. *Switched Reluctance Motor Drives: Modeling, Simulation, Analysis, Design, and Applications*. Boca Raton, Florida, USA: CRC Press, Taylor & Francis Group; 2001
- [10] Barnes M, Pollock C. Power electronic converters for switched reluctance drives. *IEEE Transactions on Power Electronics*. 1998;**13**(6): 1100-1111
- [11] Boldea I. *Variable Speed Generators*. Boca Raton, Florida, USA: CRC Press, Taylor & Francis Group; 2015
- [12] Shao B, Emadi A. A digital control for switched reluctance generators. In: *2011 IEEE International Conference on Mechatronics (ICM)*, Istanbul, Turkey. Piscataway, NJ: IEEE; 2011. pp. 182-187
- [13] Ding W. Comparative study on dual-channel switched reluctance generator performances under single- and dual-channel operation modes. *IEEE Transactions on Energy Conversion*. 2012;**27**(3):680-688
- [14] Llibre J, Martinez N, Leprince P, Nogarede B. Analysis and modeling of linear switched reluctance for medical application. *Actuators*. 2013;**2**(2):27-44
- [15] Ding W, Liang D, Tang R. A fast nonlinear variable structure equivalent magnetic circuit modeling for dual-channel switched reluctance machine. *Energy Conversion and Management*. 2011;**52**(1):308-320
- [16] Radun A. Design considerations for the switched reluctance motor. *IEEE*

Transactions on Industry Applications. September 1995; **31**(5):1079-1087

[17] Xue X, Cheng K, Ho S, Sutanto D. Precise analytical modelling magnetic characteristics of switched reluctance motor drives using two-dimensional least squares. In: 2003 IEEE 34th Annual Power Electronics Specialist Conference, PESC '03, Acapulco, Mexico. Vol. 1. Piscataway, NJ: IEEE; 2003. pp. 416-421

[18] Khalil A, Husain I. A Fourier series generalized geometry-based analytical model of switched reluctance machines. IEEE Transactions on Industry Applications. 2007; **43**(3):673-684

[19] Azongha S, Balathandayuthapani S, Edrington C, Leonard J. Grid integration studies of a switched reluctance generator for future hardware-in-the-loop experiments. In: IECON 2010—36th Annual Conference on IEEE Industrial Electronics Society, Glendale, AZ, USA. Piscataway, NJ: IEEE; 2010. pp. 3079-3084

[20] Miller T, McGilp M. Nonlinear theory of the switched reluctance motor for rapid computer-aided design. IEE Proceedings B—Electric Power Applications. 1990; **137**(6):337-347

[21] Ding W, Liang D. Modeling of a 6/4 switched reluctance motor using adaptive neural fuzzy inference system. IEEE Transactions on Magnetics. 2008; **44**(7):1796-1804

[22] Lee C. Flux linkage estimation in a switched reluctance motor using a simple reluctance circuit. Journal of Magnetics. 2013; **18**(1):57-64

[23] Filho P, Oliveira L, dos Santos Barros T, Villalva M, Filho E. Modeling and digital control of a high-power full-bridge isolated DC-DC buck converter designed for a two-stage grid-tie PV inverter. In: 2014 IEEE Energy Conversion Congress and Exposition

(ECCE), Pittsburgh, PA, USA. Piscataway, NJ: IEEE; 2014. pp. 1874-1879

[24] Miller T. Electronic Control of Switched Reluctance Machines. ser. Newnes Power Engineering Series. Oxford, UK: Elsevier Science; 2001

[25] MacMinn S, Sember J. Control of a switched-reluctance aircraft engine starter generator over a very wide speed range. In: Proceedings of the 24th Intersociety Energy Conversion Engineering Conference, 1989, Washington, DC, USA. IECEC-89. Vol. 1. Piscataway, NJ: IEEE; 1989. pp. 631-638

[26] Cardenas R, Pena R, Perez M, Clare J, Asher G, Wheeler P. Control of a switched reluctance generator for variable-speed wind energy applications. IEEE Transactions on Energy Conversion. December 2005; **20**(4):781-791

[27] Rain X, Hilairet M, Bethoux O. Comparative study of various current controllers for the switched reluctance machine. In: 2010 IEEE Vehicle Power and Propulsion Conference, Lille, France. Piscataway, NJ: IEEE; 2010. pp. 1-6

[28] Choi D, Byun S, Cho Y. A study on the maximum power control method of switched reluctance generator for wind turbine. IEEE Transactions on Magnetics. 2014; **50**(1):1-4

[29] Mademlis C, Kioskeridis I. Optimal efficiency control of switched reluctance generators. IEEE Transactions on Power Electronics. 2006; **21**(4):1062-1072

[30] Pan J, Yu Z, Cheung N, Guang-Zhong C. On the voltage ripple reduction control of the linear switched reluctance generator for wave energy utilization. IEEE Transactions on Power Electronics. 2014; **29**(10):5298-5307

[31] Hasanien H, Muyeen S. Speed control of grid-connected switched reluctance generator driven by variable speed wind turbine using adaptive neural network controller. *Electric Power Systems Research*. 2012;**84**(1): 206-213

[32] Babarit A, Hals J, Muliawan MJ, Kurniawan A, Moan T, Krokstad J. Numerical benchmarking study of a selection of wave energy converters. *Renewable Energy*. 2012;**41**(0):44-63

IntechOpen